June 2003 • NREL/SR-520-34314

Subcontractor Report

Tolerance of Three-Stage CIGS Deposition to Variations Imposed by Roll-to-Roll Processing

Phase I Annual Report
May 2002–May 2003

M.E. Beck
Global Solar Energy, Inc.
Tucson, Arizona

I.L. Repins
ITN Energy Systems, Inc.
Littleton, Colorado

National Renewable Energy Laboratory

1617 Cole Boulevard
Golden, Colorado 80401-3393

NREL is a U.S. Department of Energy Laboratory
Operated by Midwest Research Institute • Battelle • Bechtel

Contract No. DE-AC36-99-GO10337

June 2003 • NREL/SR-520-34314

Tolerance of Three-Stage CIGS Deposition to Variations Imposed by Roll-to-Roll Processing

Phase I Annual Report
May 2002–May 2003

M.E. Beck
Global Solar Energy, Inc.
Tucson, Arizona

I.L. Repins
ITN Energy Systems, Inc.
Littleton, Colorado

NREL Technical Monitor: H.S. Ullal

Prepared under Subcontract No. ZDJ-2-30630-14

National Renewable Energy Laboratory

1617 Cole Boulevard
Golden, Colorado 80401-3393

NREL is a U.S. Department of Energy Laboratory
Operated by Midwest Research Institute • Battelle • Bechtel

Contract No. DE-AC36-99-GO10337

NOTICE

Available electronically at http://www.osti.gov/bridge

Available for a processing fee to U.S. Department of Energy
and its contractors, in paper, from:

U.S. Department of Energy
Office of Scientific and Technical Information
P.O. Box 62
Oak Ridge, TN 37831-0062
phone: 865.576.8401
fax: 865.576.5728
email: reports@adonis.osti.gov

Available for sale to the public, in paper, from:

U.S. Department of Commerce
National Technical Information Service
5285 Port Royal Road
Springfield, VA 22161
phone: 800.553.6847
fax: 703.605.6900
email: orders@ntis.fedworld.gov
online ordering: http://www.ntis.gov/ordering.htm

Printed on paper containing at least 50% wastepaper, including 20% postconsumer waste

TABLE OF CONTENTS

LIST OF FIGURES

LIST OF TABLES

1 Introduction

1.a Background

Co-evaporation of $CuIn_xGa_{1-x}Se_2$ (CIGS) via two-stage and three-stage processes has been used in a variety of laboratories throughout the world to produce small-area devices with efficiencies greater than 15%.[1,2,3,4,5] Thus, these deposition methods have come to be viewed as laboratory standards for the formation of CIGS absorbers used in respective photovoltaic (PV) devices. Although quite successful and relative easy to implement on a small R&D scale, scale-up to a commercially viable level proves to be rather challenging, as a number of conditions are encountered during continuous manufacturing that differ from the laboratory process. Such differences include both those imposed by continuous processing of moving substrates, and those implemented to decrease costs and increase throughput. It is therefore beneficial to understand the tolerance of the established laboratory processes to variations in deposition procedures.

Only limited information is available in the literature addressing the tolerance of the laboratory processes to several variations. Published studies are limited to CIGS thickness,[6] maximum deposition temperature and time spent by the film in the Cu-rich stage,[7,8] Na content,[9,10] and final overall Cu/(In+Ga) atomic ratio.[11] Not only are there additional, at times more important, absorber characteristics that define the quality of the resulting absorber for use in a PV device, but these experiments were conducted without correlation to practical commercial fabrication methods. Further variations to the deposition procedure may be encountered in the manufacturing environment and include:

- Deviation of initial film temperature from the prescribed two- and three-stage values,
- Variation in the fraction of group III elements deposited in the first versus third stages,
- Instantaneous variations in the Se/metals flux ratio outside the typically-recommended envelope due to spatial distribution of metallic flux,
- Further shortened overall deposition times,
- Variations in sample cool-down rate and Se flux during cool-down,
- Impurities expected from less expensive, less pure source materials or alternative substrates,
- Exposure to species outgassed and reflected from hot chamber walls, and,
- Exposure to air (oxygen and humidity) after CIGS deposition for varying amounts of time followed by varying CdS deposition techniques.

Global Solar Energy, Inc. (GSE) and lower-tier subcontractor ITN Energy Systems, Inc. (ITN) are addressing these process tolerance issues in this program. The definition and resolution of process tolerance issues satisfy many of the goals of the Thin Film Photovoltaics Partnerships Program (TFPPP). First, the investigation is likely to identify acceptable ranges for critical deposition parameters. This will have the benefit of providing upper and lower control limits for in-situ process monitoring components, thus increasing average efficiency as well as yield of product. Second, the exploration may uncover insensitivities to some processing procedures, allowing manufacture of modules at increased throughput and decreased cost. The exploration allows a quantitative evaluation of the trade-offs between performance, throughput, and costs. Third, the proposed program also satisfies the TFPPP goal of establishing a wider research and development base for higher-efficiency processing. Fourth, the acquisition of data defining sensitivity to processing has important implications for the required accuracy of process sensors and control. Finally, the program helps the photovoltaic community advance toward a better understanding of CIGS growth, a longer-term goal of the TFPPP.

1.b Definition of Technical Scope

Two-stage and three-stage processes laboratory CIGS depositions are batch processes where deposition fluxes and temperatures are varied with time. Temperature and flux profiles for the two-stage[2] and three-stage[1] processes are shown in Figure 1 and Figure 2. These depositions are generally performed in cold-wall reactors with very low base pressures.

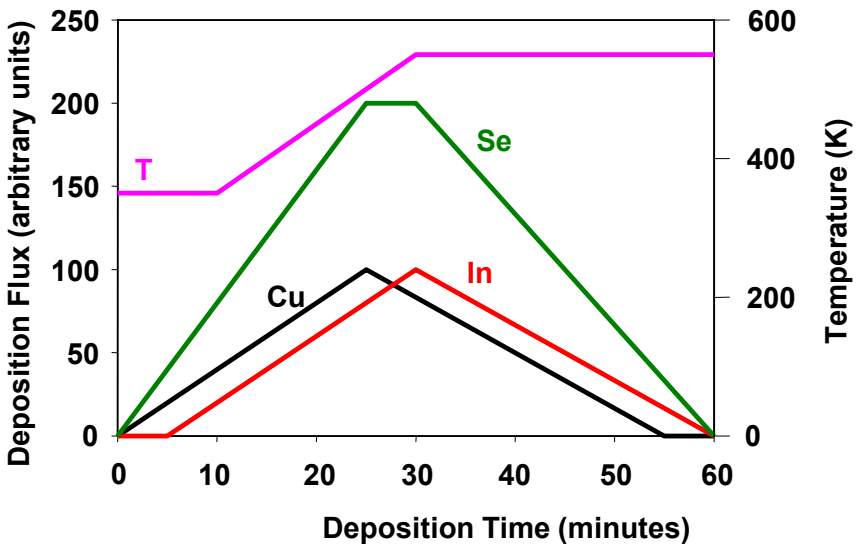

Figure 1: Temperature and flux profiles for two-stage CIGS deposition process.

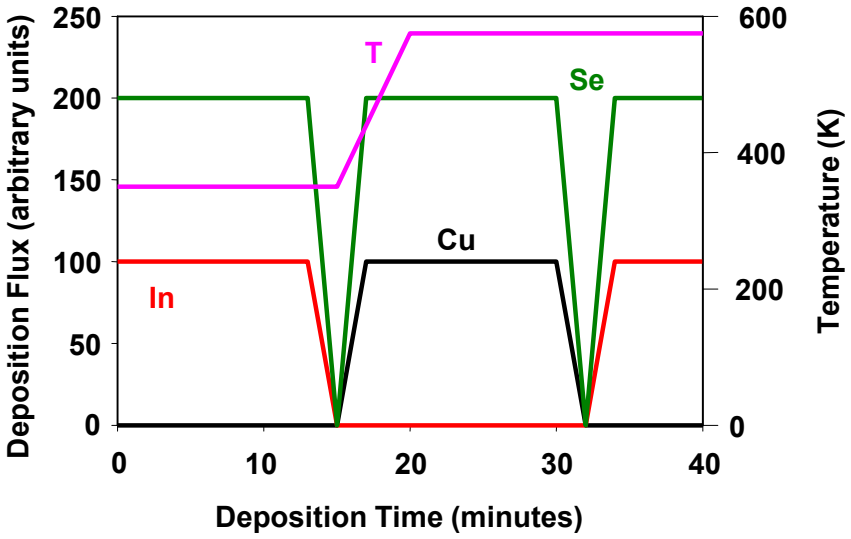

Figure 2: Temperature and flux profiles for three-stage CIGS deposition process.

Processing moving substrates (i.e., dynamic depositions) does not allow for exact replication of the flux and temperature profiles depicted in Figure 1 and Figure 2 for static substrates. The delivery of Cu, In, and Ga follows a cosine-type distribution, rather than the flatter profiles of the above graphs. Also, since evaporation sources must be placed close enough to the substrate to provide reasonable materials utilization, yet far enough apart to allow independent control of each source and substrate temperature, the different metallic fluxes tend to be separated in time more than those of the laboratory process. As an illustration, Figure 3a shows the calculated flux profiles from a effusion source with cosine-based distributions. The calculations were made using a spreadsheet developed at the Institute for Energy Conversion (IEC). The source arrangement of Figure 3 attempts to imitate the two-stage recipe, depositing a Cu-rich film that is brought back to stoichiometry and near the end of the deposition crosses into a slight Cu-poor regime. However, the spatial separation

between the sources causes the film to be much more Cu-rich during most of the dynamic deposition than is the case during the laboratory two-stage process illustrated in Figure 1. Figure 3b shows the instantaneous and cumulative Cu/(In+Ga) ratios as a function of time (or distance) for the dynamic deposition.

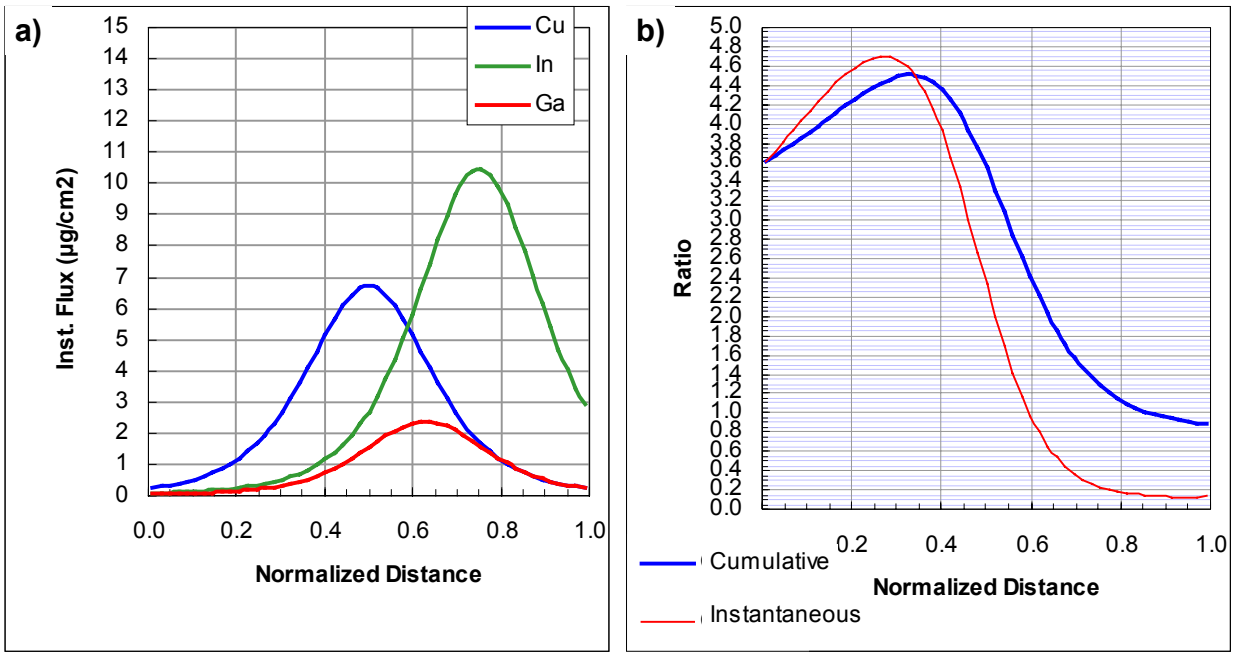

Figure 3: Calculated flux profiles and Cu/(In+Ga) ratio as a function of distance for deposition onto moving substrate.

The relatively sharp increases and decreases in metal fluxes seen by the sample, as in Figure 3a, has implications for the Se to metals ratio as well. During typical laboratory depositions, the Se flux is kept in excess with respect to the combined metal fluxes in the range of 2 to 6 times. The sharp profiles of Figure 3b imply that unless Se distribution is precisely tuned to the metal profiles, the sample is likely to experience periods where Se flux outside the typically-recommended 2× to 6× envelope.

Replication of the temperature profiles of the laboratory processes can also be problematic. The temperature profile experienced by a sample during continuous manufacturing depends not only on heater temperatures in different zones, but also on the thermal mass of the moving sample, the speed at which the sample moves, the thermal conductivity and emissivity of the sample, and evaporation source temperatures. As an example, the black line in Figure 4 shows calculated substrate temperature profile under the baseline conditions during roll-to-roll (RTR) CIGS deposition. In comparison, the green line shows the temperature profile when the evaporation sources are turned off. As is evident from these two lines in the plot, the evaporation sources can be expected to have a significant contribution to substrate heating. Were the heat capacity of the substrate increased by a factor of 10×, the blue line plotted in Figure 4 describes the effect on substrate temperature for this scenario. Hence, the heat capacity of the sample is very important to the temperature profile it experiences, as it controls how quickly the sample temperature reacts to changes in the surroundings. The red line shows the temperature profile experienced by a sample with even higher heat capacity: a 1/8" piece of glass. Finally, the yellow line shows the effect of assigning a variable emissivity to the web based on the film composition. Relative changes in emissivity were inferred from Kessler et al.[12]

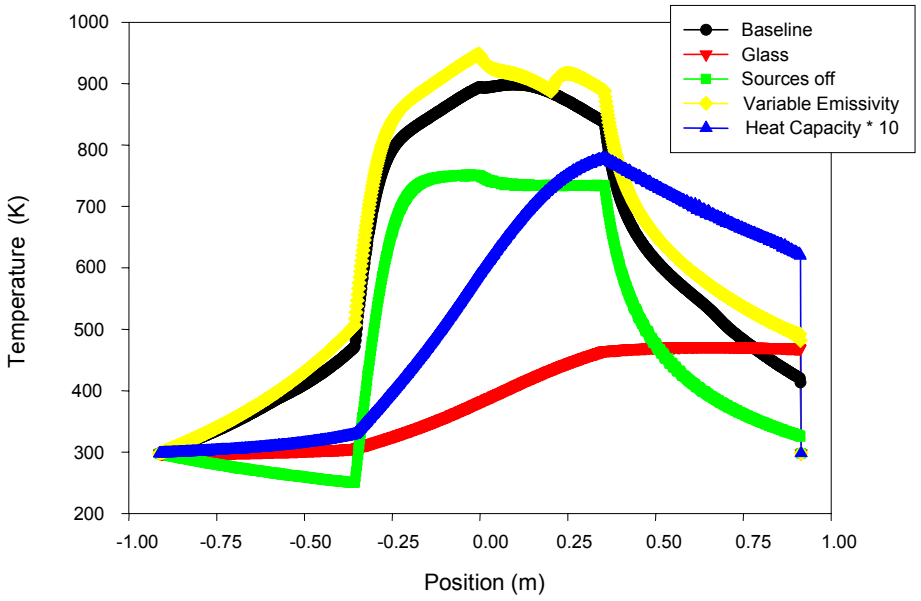

Figure 4: Calculated temperature profiles (^{o}K) for a variety of variations from baseline conditions.

Differences between the laboratory and manufacturing processes are also encountered in exposure during deposition to species outgassed and reflected from hot chamber walls. Such differences are difficult to avoid considering the differences in sample areas from the laboratory to the production environment. In the laboratory, the sample and the heated area is much smaller than the chamber. Thus the chamber walls remain relatively cool, and species evaporated onto the chamber walls do not return to the deposition zone. In production, the same size scale between the substrate area and chamber size cannot be maintained without unreasonable vacuum equipment size and costs. As a consequence, the sample and heated deposition zone occupy a much larger fraction of the chamber. The difference in heated fractions of the chamber between the laboratory and production scale is shown schematically in Figure 5. The red areas represent hot portions of the chamber, and the blue areas represent cool portions of the chamber. This illustrates that the laboratory process is essentially a cold-wall evaporation, while the production process represents a hot-wall evaporation. Not only is the production deposition subject to species outgassed and reflected from the hot walls, but the lack of relatively cool and low-Se areas precludes the use of traditional flux sensors that must operate at low temperatures, such as quartz crystal microbalances (QCM) and electron impact emission spectroscopy (EIES).

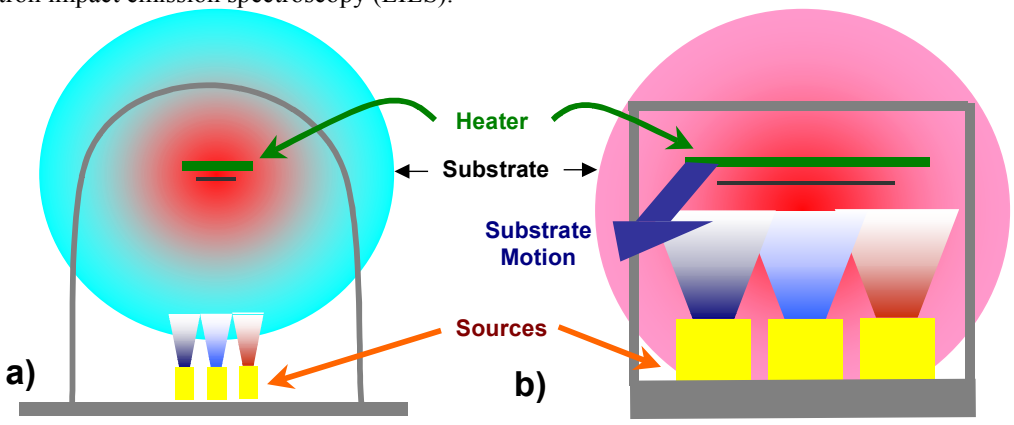

Figure 5: Schematic representation of heated area and chamber are for a) laboratory and b) production CIGS deposition.

Besides these inherent differences, some modifications to the three-stage process are desirable in manufacturing simply to decrease costs. For example, shortened overall deposition time increases throughput. Also, purchase of source materials with higher impurity levels (for example, 99.9% purity instead of 99.999% purity) decreases feedstock costs.

Roll-to-roll manufacturing on thin, light-weight, flexible substrates imposes further variations to the three-stage process method. For example, fundamental differences exist due to the choice of substrate and impurity out-diffusion, surface roughness of metallic substrates, temperature stability of polymeric substrates, differences in heat capacity need to be accounted for in the choice of deposition parameters. Hence, if a flexible sample is not heated beyond the deposition zone, it cools more rapidly than the rate prescribed in the three-stage recipe. It also may be exposed to varying amounts of Se during the cool-down. Furthermore, in the three-stage process, 90% of the In and Ga is typically deposited during the first stage, with the remainder deposited in the third stage.[11] In production, it is desirable to vary the ratio of first-stage to third-stage In significantly from the 90%/10% split to address adhesion and source-control issues. In combination with faster deposition rates, the latter has significant implications on the reaction kinetics and diffusion profiles. Finally, although the deposition of window layers is generally less complicated than that of the CIGS, the performance of window layers is also affected by throughput and continuous processing considerations.

1.c Approach

The approach to address the issues mentioned above consists of four basic parts:

1. Setting up the NREL-developed three-stage laboratory process in a bell jar at ITN.
2. Characterizing the RTR production chambers at GSE in terms of the important variables.
3. Using the bell jar system to step from the NREL process to the conditions experienced by a sample during roll-to-roll manufacturing, and characterizing the resulting films – i.e., simulation of a dynamic process in a static environment.
4. Utilizing the process sensitivity information gained in the bell jar system in the production chambers.

These four tasks are being performed roughly in the order listed. During Phase I, a three-stage bell jar process was established at ITN, the GSE RTR production processes were characterized in terms of several important variables, and the bell jar system was used to explore some sensitivities of the three-stage process that are applicable to the production environment. During Phase II, it is expected that the important deposition conditions in the production chambers will be fully specified, and the sensitivity of the three-stage process to each of these conditions will be investigated in the bell jar. Progress on each Phase I task is described in following sections.

2 Bell Jar Baseline

To explore process sensivitivies, the NREL-developed three-stage CIGS deposition process has been established in a 22” bell jar. Metals and Se fluxes are under closed-loop control via electron impact emission spectroscopy (EIES) and quartz crystal microbalance (QCM), respectively. Radiative substrate heating is monitored by contact and ambient thermocouples. A thermopile is used for compositional endpoint detection. For maximum reproduciblity, process setpoints and times are executed by computer-programmed recipes, and monitored quantities are automatically logged.

Many aspects of establishing this baseline process have proceeded favorably. CIS composition is repeatable from run to run, and 1 cm^2 total area devices up to 9.3% efficiency (without anti-reflection (AR) coating) are produced, with reasonable uniformity over the 3” × 3” substrate. For example, across the 50 CIS devices on substrate B020822, average device efficiency was 7.9%, with a mimimum and maximum efficiency of 6.8% and 8.7%, respectively . Quoted efficiencies are total-area, AM1.5, for 1 cm^2 devices, without AR coating or Ga. Best CIS efficiency achieved in the bell jar on 0.001” thick production steel is 7.7%. Current-voltage (JV) curves for the best CIS devices from the bell jar on glass and 0.001” steel are shown in Figure 6, with device parameters listed in the inset.

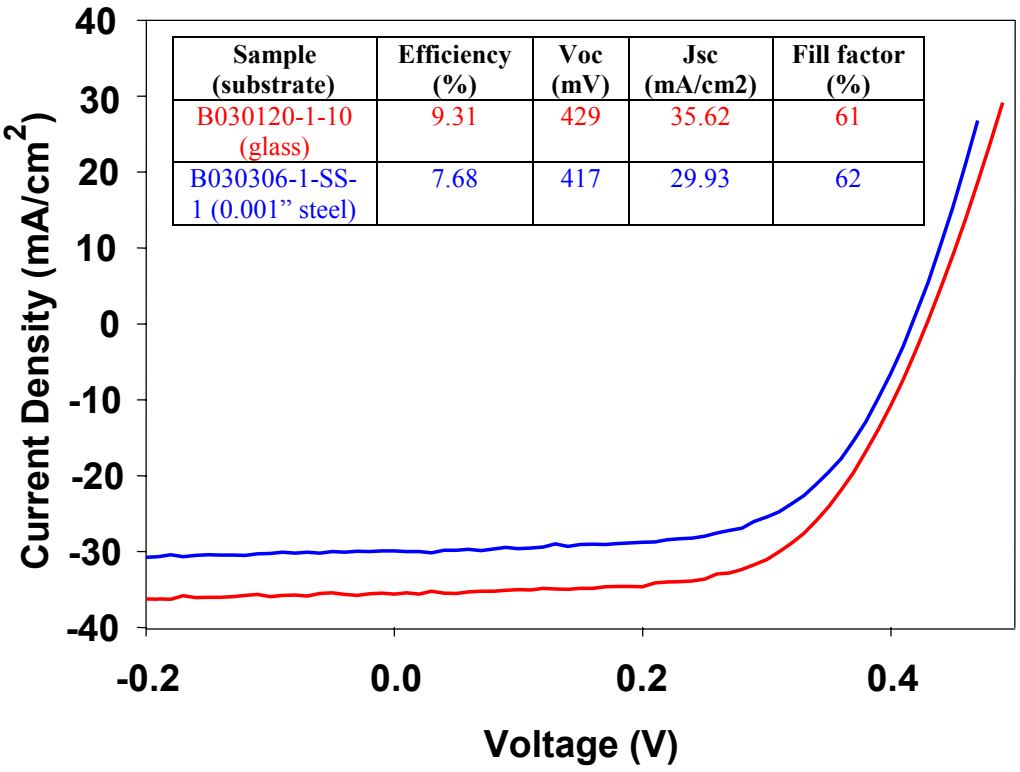

Figure 6: JV curves for most efficient CIS devices on glass and 0.001" steel.

Reaching this level of performance required fine-tuning several of the equipment components. First, higher wattage heater bulbs were installed to allow temperature setpoints to be achieved in times much shorter than each process stage. Also, proportional-integral-derivative (PID) control parameters on each evaporation source were tuned for optimum control. Cooling lines were installed along the tube from the EIES filament to the EIES signal window, to prevent coating the window with Se. Extra light shielding was installed around the substrate heater lamps to prevent the Se QCM from overheating, and to prevent creating false signal in the EIES detector.

Further improvements have been required for reproducible incorporation of Ga into the film. Including Ga in the deposition makes processing more difficult for two reasons: 1) Due to the small amount of Ga to be incorporated into the film and the tendency of Ga atoms to emit light only weakly from excited atomic states, the Ga rate on the EIES is the weakest and hence noisiest of all the film constituents. 2) It was found – as described in section 4.a , "Importance of Cu-rich stage" – that for CIGS films, device performance is more sensitive to the presence of a Cu-rich stage than are CIS films. Thus, a higher resolved in-situ control of not just the end composition, but also the composition at the end of the second stage, is required. Several steps were taken to achieve reproducible deposition of high-quality Ga-containing films. Evaporation sources and EIES signal beam splitters were rearranged to maximize the weak Ga signal. A pre-deposition bakeout was implemented to minimizes transient noise that otherwise occurs in the electron impact emission spectrometer (EIES) Ga rate reading when deposition temperature is increased to 550°C and surfaces outgas. A robust EIES calibration procedure performed before every run was also established. The resulting logged fluxes and temperatures versus time for a typical CIGS run are plotted in Figure 7. Finally, successful procedure to utilize the CIGS emissivity change via an infrared (IR) sensor was established, as described below.

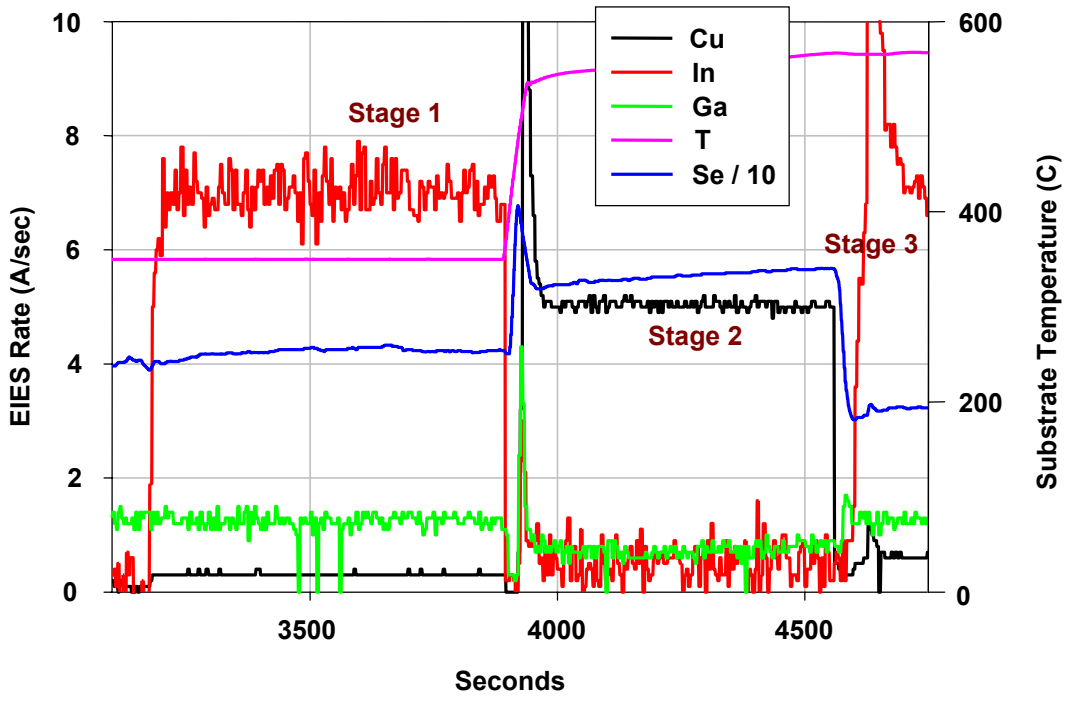

Figure 7: Logged fluxes and temperatures for a typical baseline CIGS run (#B030501-1).

CIGS emissivity is higher when Cu-rich than when Cu poor.[12,13,14,15] Thus, monitoring the CIGS emissivity allows fine control the extent of the Cu-rich excursion and the final composition. Such monitoring is usually performed using a contact thermocouple, and noting – as emissivity increases – either a decrease in temperature at constant power, or an increase in power to maintain a constant temperature. Monitoring emissivity via contact thermocouple can be problematic for several reasons. First, depending on system parameters, the expected temperature change may be only a fraction of a degree C. Furthermore, power and temperature fluctuations can mask the effect, as temperature is controlled despite the thermal influence of the deposition sources. Most important, for flexible substrates that either have a low thermal mass or cannot sustain the mechanical pressure of a thermocouple, the method cannot be applied.

Suitable contactless means of obtaining this critical information include (laser) light scattering or IR sensing instruments. IR monitoring of the substrate was choosen and found to provide unambiguous detection of the Cu-poor to Cu-rich transition, as well as the transition back from Cu-rich to Cu-poor. A thermopile was installed in the bell jar12" from the substrate. Optics collect emission from approximately a 1" diameter spot on the substrate, over a 6 to 14 μm wavelength range. The sensor coats gradually over 10's of depositions. However, as the identifying the emissivity change requires only a relative measurement, slow coating does not affect the sensor efficacy.

To recognize the CIGS emissivity transitions from an IR sensor, it is necessary to understand how the emission from the substrate evolves throughout the deposition. The progression of the IR signal through a CIGS deposition is illustrated qualitatively in Figure 8. Both CIGS and In_2Se_3 are largely transparent in the IR. Thus, as the film grows, interference fringes move in and out of the thermopile wavelength band, and the thermopile signal oscillates with time. (The appearance of interference fringes in CIGS and In_2Se_3 emissivity was demonstrated and explained in DOE contract DE-FG03-02ER83472/A000 "Non-Contact Temperature and Emissivity Sensor for Lower-Cost CIGS Photovoltaics Manufacturing". Details will be published as part of that project if Phase II SBIR support is received.) Figure 8a therefore shows the IR signal from a growing film at constant temperature, as a function of time. IR emission increases with temperature, so, if a temperature step is included in the deposition, a signal like that shown in Figure 8b results. If a period of increased emissivity is included in the deposition, emission during that time period is larger, and a signal like that shown in Figure 8c is expected.

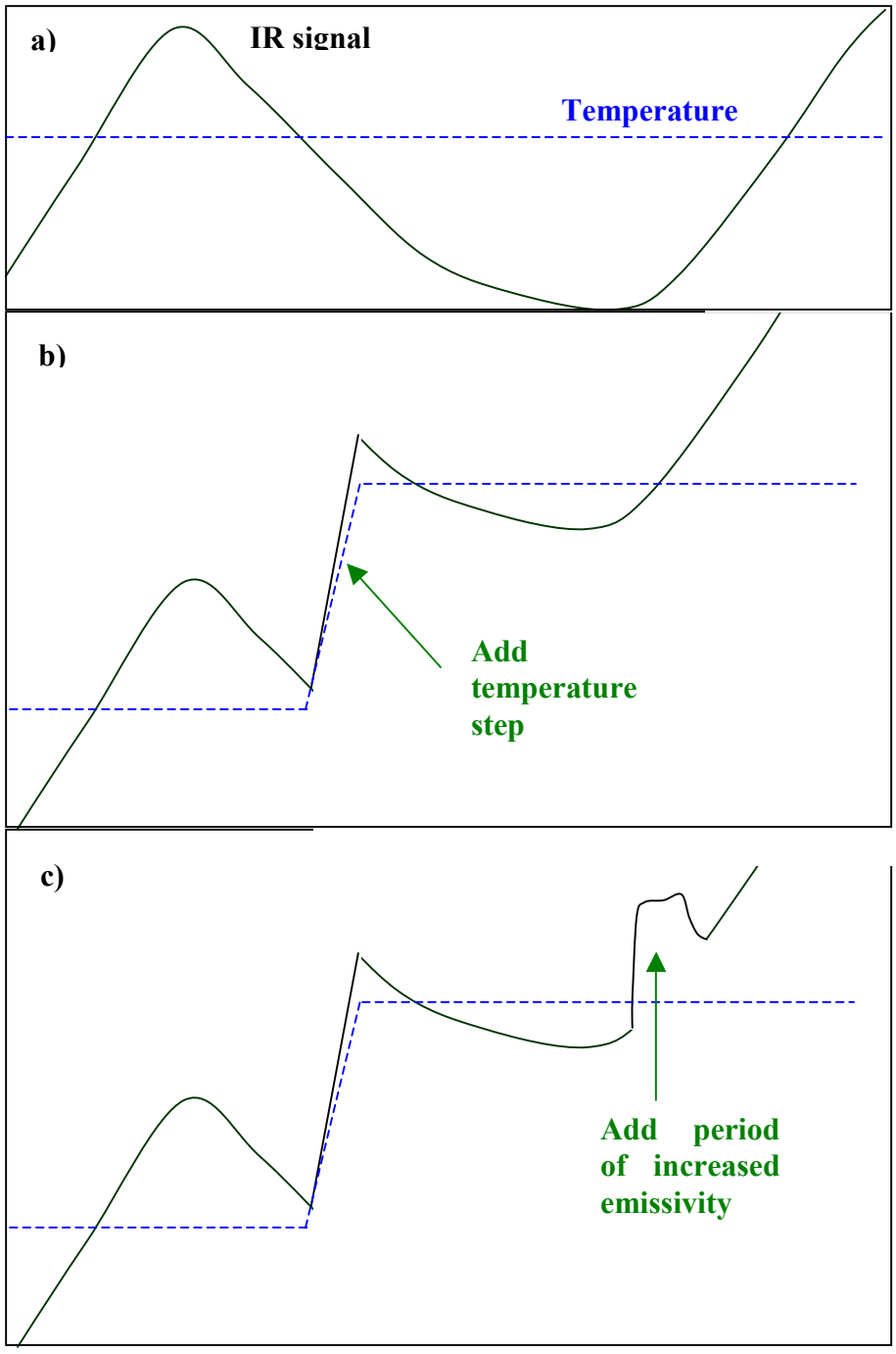

Figure 8: IR signal from growing CIGS film a) at constant temperature, b) with temperature step, and c) with temperature step and emissivity change.

Figure 9 shows measured IR data from a CIGS deposition, superimposed on flux and temperature data. The expected features illustrated in the previous paragraph are noted.

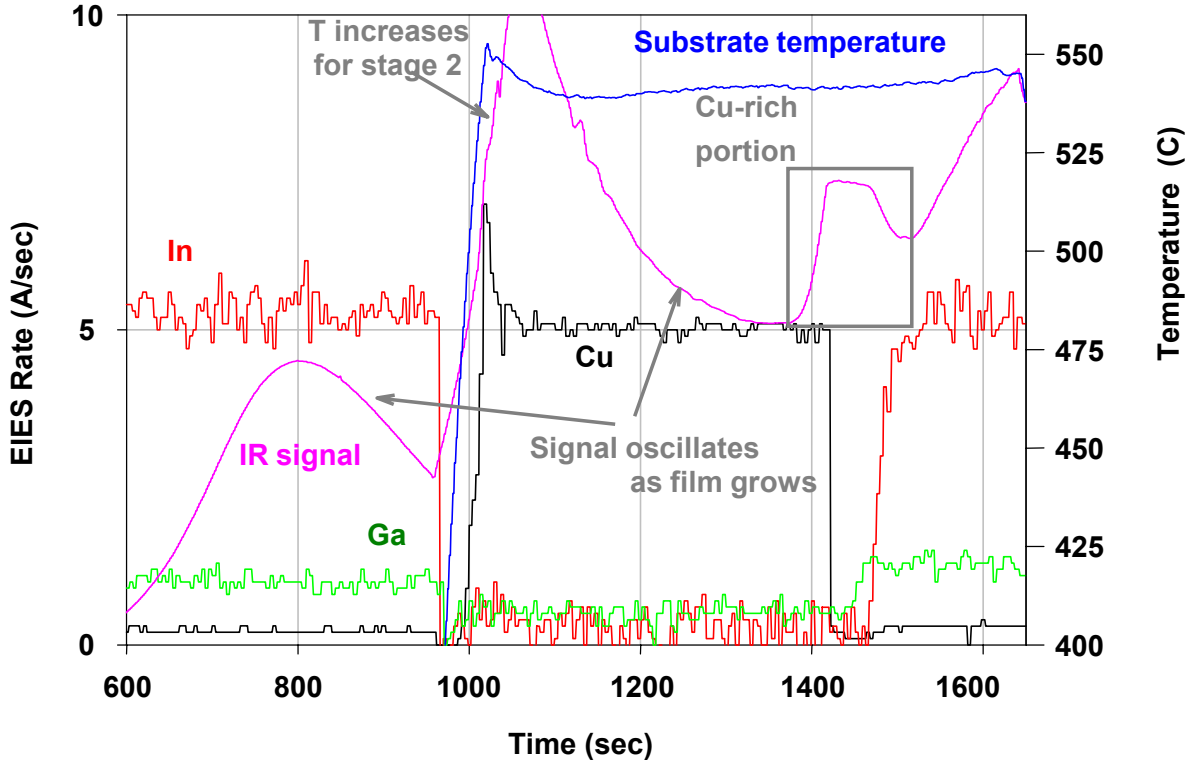

Figure 9: IR data from CIGS run 030516-1.

As expected, the incorporation of Ga into the devices increases device efficiency due to a better match of the absorber bandgap to both the solar spectrum and the indium tin oxide transmission. The number of devices made containing Ga has been limited compared to those made with CIS, due to the extra considerations for Ga described in the previous paragraphs. However, over this limited number of CIGS samples, 10.9% efficiency has been demonstrated and it is expected that the quality of devices with Ga will increase slightly as the emissivity change is incorporated into the processing procedure.

Buffer and window layers regularly deposited on CIGS from the bell jar were determined to be of good quality. Two halves of the same absorber were finished into devices both at ITN and at NREL. Resulting efficiencies were nearly identical. ITN devices showed very slightly lower short-circuit current and higher fill factor, possibly due to a slightly more conductive but darker transparent conducting oxide.

3 Roll-Coater Conditions

A second major task under this program is characterizing the roll-to-roll production chambers at GSE in terms of the variables known to be important to the three-stage process. For CIGS deposition, those variables include substrate temperature as a function of time, as well as Cu, In, Ga, and Se fluxes as a function of time. Also important to final device efficiency are the quality of the window layers. Status of the examination of each of these quantities during Phase I is described in the sub-sections below.

3.a Metals flux profiles

Processing moving substrates (i.e., performing dynamic depositions) does not allow for exact replication of the flux and temperature profiles of the laboratory three-stage process. As the substrate moves over the evaporation sources, the delivery of Cu, In, and Ga follows a cosine-type distribution, rather than the flatter flux vs. time profiles typical of the static laboratory three-stage process. Also, since evaporation sources must be placed close enough to the substrate to provide reasonable materials utilization, yet far enough apart to allow independent control of each source and substrate temperature, the different metallic fluxes tend to be separated in time more than those of the laboratory process. Effusion source profile data was gathered as described below.

The Cu effusion source profile was measured in the "Intelligent Processing" (IP) roll-to-roll (RTR) CIGS coater at ITN. This chamber contains a version of the GSE production effusion sources, and is pictured in Figure 10. The experiment geometry is shown in Figure 11, and the following steps were taken:

1. The Cu source was warmed up to the desired temperature setpoint.
2. Clean web was advanced forward into the deposition zone at maximum speed.
3. The web was held stationary over the source for 3 minutes.
4. The coated web was then advanced forward out of the deposition zone at maximum speed.
5. Subsequently the web was removed from the chamber, and a down-web strip was cut out of the web. Ex-situ x-ray fluorescence (XRF) measurements were made at increments of 0.5" to 1" on the down-web strip, over a distance of 30".

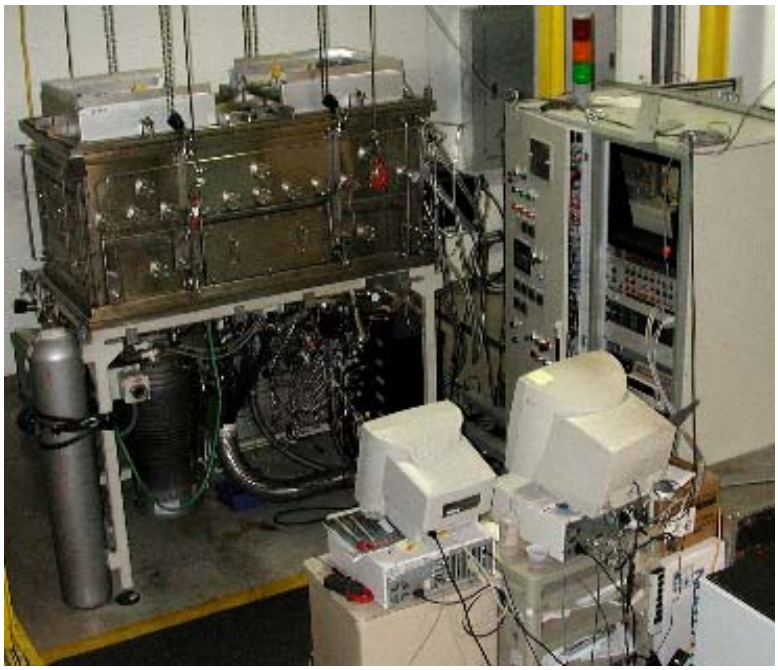

Figure 10: IP roll-to-roll CIGS chamber at ITN.

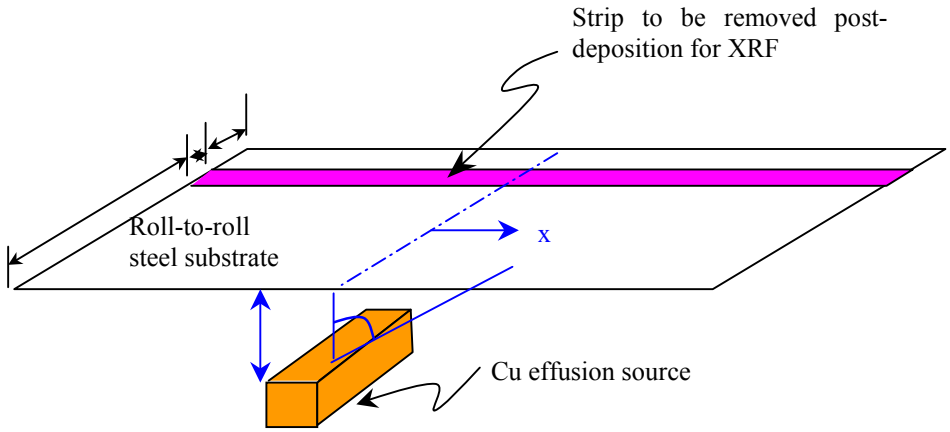

Figure 11: Geometry and coordinate system used for effusion source profile measurement.

The resulting Cu thickness as a function of down-web position on the strip is shown in Figure 12. As mentioned, quoted thickness values were obtained by XRF and the data is plotted on a log scale to allow better viewing of the amount of noise in the lower thickness points. Measurement scatter is in the 10's of angstroms range and the 200 Å offset between the x-axis and the Cu thickness far from the effusion source represents the amount of Cu deposited when the web was moved in and out of the deposition zone at the maximum transport speed.

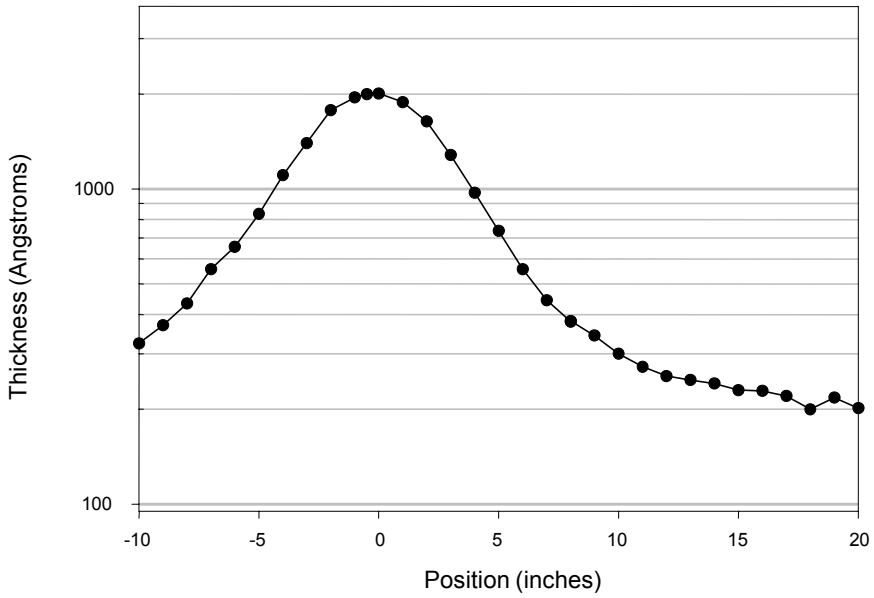

Figure 12: Cu thickness as a function of down-web position, plotted on log scale.

The Cu profile above is found to agree well with a $\cos^3\theta$ dependence of the flux per solid angle. To make the comparison, geometry factors that convert the distribution from a function of θ to a function of x were included. The results are shown, both on linear and log scales, in Figure 6. The fit assumes 200 angstroms were deposited while advancing the web (as mentioned in the previous paragraph), and the overall magnitude of the effusion rate was scaled to match the measured rate at x = 0. The difference between the fit and measured points is negligible compared to the difference between the roll-coater flux profile and the laboratory three-stage flux profile.

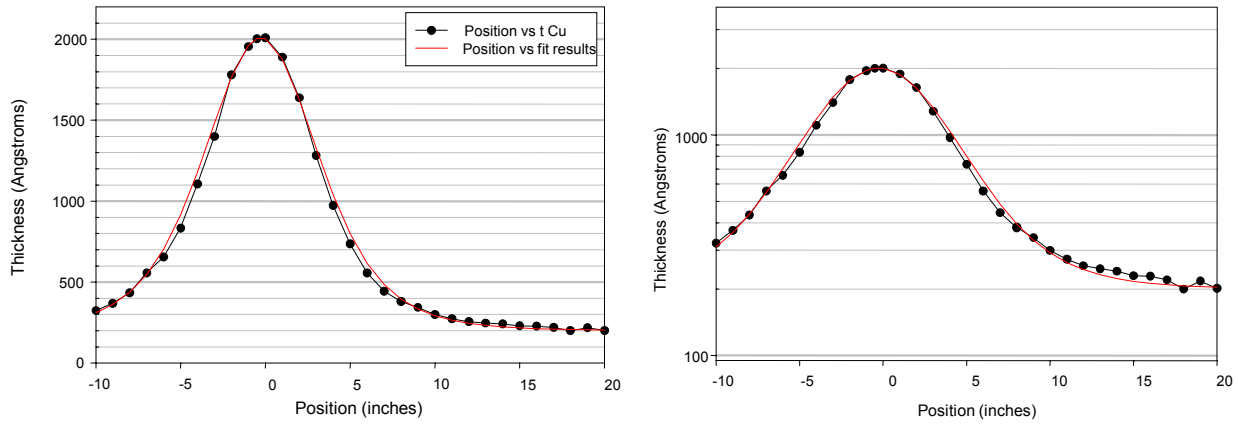

Figure 13: Cu thickness as a function of down-web position compared with $\cos^3\theta$ fit, plotted on linear (left) and log scales (right).

This $\cos^3\theta$ dependence of effusion source distributions has also been measured at the Institute for Energy Conversion (IEC).[16] IEC reports no dependence of the profile on source metal, and no dependence on deposition rate over a 100× range of deposition rates. Thus – when combined with information on effusion source placement, source-to-substrate distance, substrate speed, and rate of material leaving the source – the $\cos^3\theta$ distribution is an adequate starting point to define the roll-coater metals flux profiles for the bell jar experiments.

3.b Effect of Se on metals flux profiles

The previous section described metals flux profiles from manufacturing effusion sources operated in the absence of Se flux. Monte Carlo modeling performed at the Colorado School of Mines indicates that a background pressure of Se may significantly affect the metals profiles under normal CIGS deposition conditions.[17] Thus, preparations are underway to repeat the experiments described in the previous section in the presence of several different Se rates. Currently, a hot containment zone is being installed in the IP chamber (Figure 10) in order to both emulate the hot-wall environment of lengthy production runs, and to insure that Se is well-defined during the flux profile examinations.

3.c CdS bath uniformity

Studies also have been conducted to investigate process parameter sensitivity in aqueous CdS deposition. One aspect of these studies is the solution temperature as a function of time and position. Figure 14 illustrates IR temperature maps in a CdS reaction vessel before and after modifications to improve temperature uniformity. A thermograph of the CdS bath shortly after addition of solution is shown in Figure 14a. The highlighted 3" × 3" area is characterized by a temperature minimum of 48.6°C, a maximum of 83.9°C, and an average ± 1σ of 59.3 ± 7.6°C. The center point is at 51.2°C. In Figure 14b, the highlighted 3" × 3" area is characterized by a temperature minimum of 61.5°C, a maximum of 69.0°C, and an average ± 1σ of 64.4 ± 1.4°C. The center point is at 62.9°C.

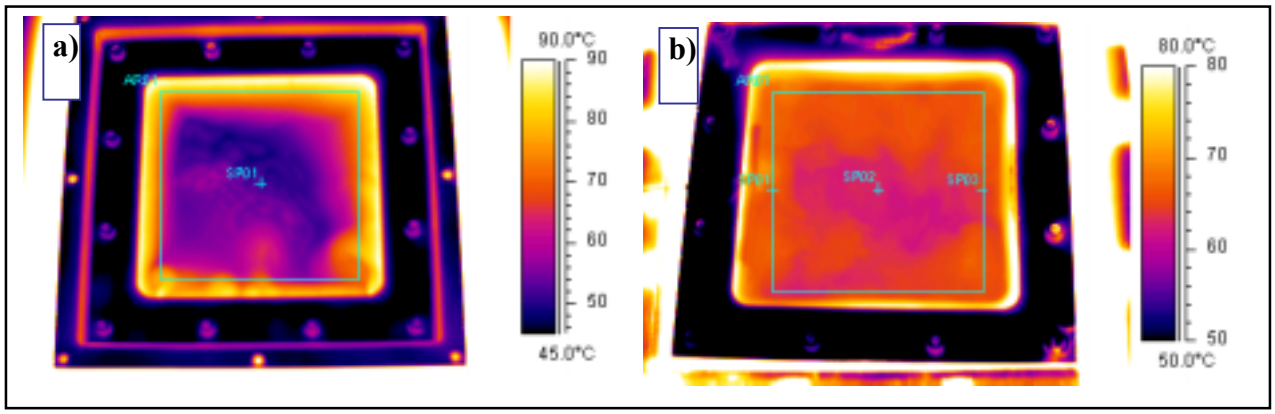

Figure 14: IR photos of CdS reaction vessel a) before and b) after modifications for temperature uniformity.

Furthermore, an examination into the effects of various Cd treatments on the CIGS surface is underway with the cooperation of researchers at NREL and University of Illinois. Data will be available after patent considerations have been fully assessed.

3.d Window layer performance

The preceding sub-sections have focused on tolerance of the CIGS process only. It is also important, of course, to manufacture devices with buffer and window layers optimized within an acceptable envelope, and to understand the contribution of the window layers toward efficiency loss and variability. One step toward this goal is establishing the level of performance of the GSE baseline layers compared to trusted laboratory standards. Thus, a comparison of small area (0.68 cm^2) device performance based on GSE SS/Cr-Mo/CIGS samples finished at GSE, NREL, and IEC was carried out. James Keane at NREL performed CBD CdS and i-ZnO/Al_2O_3:ZnO depositions, and Bill Shafarman at IEC coordinated CBD CdS and i-ZnO/ITO depositions there.

Table 1 shows the matrix for device finishing. All samples were retrieved and randomized from a 30 ft. section of CIGS (lot 831SB), previously screened at the diode level to ensure uniform material properties. To accommodate throughput limitations at both IEC and NREL, the number of replicas indicated in Table 1 was reduced to as few as two samples per condition. Each sample represents a 3" × 3" diode array consisting of 50 0.68 cm^2 devices. GSE CdS buffer layers were deposited in the second half of September 2002, using both a high-throughput (HT) and lower-throughput (LT) CdS process. The last set of CBD CdS coated coupons from NREL were received in early February 2003. Subsequently, all samples requiring GSE window layers were i-ZnO:ITO coated in one run (970SA). Device isolation into 0.68 cm^2 diodes was accomplished via laser scribing, and an e-beam evaporated Ag grid completed the test structure. All device parameters reported are under AM1.5 conditions at 25°C. Prior to statistical analysis, each set was filtered removing devices with parameters deviating from the normal distribution at the 95% confidence level.

# Samples	Layer(s) at GSE	Layer(s) at NREL	Layer(s) at IEC
6	HT CdS	i-ZnO/2%Al_2O_3:ZnO RF sputtered	
6	LT CdS	i-ZnO/2%Al_2O_3:ZnO RF sputtered	
6	HT CdS		i-ZnO/ITO
6	LT CdS		i-ZnO/ITO
4	i-ZnO/ITO	CBD CdS	
4	i-ZnO/ITO		CBD CdS
4		CBD CdS/i-ZnO/2%Al_2O_3:ZnO	
4			CBD CdS/i-ZnO/ITO
4	HT CdS/i-ZnO/ITO		
4	LT CdS/ i-ZnO/ITO		
4		CBD CdS	i-ZnO/ITO
4		i-ZnO/2%Al_2O_3:ZnO	CBD CdS

Table 1: Design of Experiment matrix listing all permutations for buffer and window layer device completion between GSE, ITN, and NREL.

Figure 15 summarizes the estimated effects on device parameters of varying buffers or windows as compared to the standard GSE process. Several features are worth noting. First, efficiency values in Figure 15a indicate that both the September 2002 GSE HT CdS and LT CdS are superior to the other buffers in this study. It is not known what fraction of that advantage is due to CdS processing variables, and what fraction may be due to changes in the CIGS sample occurring during shipping to or storage at IEC and NREL. Second, it should also be noted that the GSE HT CdS does not quite reach the performance of the GSE LT CdS layer: the higher throughput in this experiment comes at some cost to efficiency. Subsequent changes to correct this situation have been made to the HT CdS process and are under evaluation. Third, with respect to the window layers, the IEC i-ZnO/ITO outperformed both the GSE i-ZnO/ITO as well as the NREL i-ZnO/Al_2O_3:ZnO, mostly due to a slightly enhanced fill factor compared to the GSE process. The highest efficiency combination is a GSE LT CdS with an IEC window. The GSE window layer nevertheless performs well on the NREL, IEC and GSE LT CdS buffers. These window layer comparisons can be seen most clearly by examining Figure 16. The latter shows device parameters measured on each permutation of buffer and window layer combinations. Finally, Figure 15b and Figure 16 indicate a substantially reduced current and voltage from some NREL samples. As this reduction is not present for the other specimens that traveled in between buffer and window deposition at IEC, NREL, and GSE, transport damage can be excluded. It is possible that the NREL window is not matched to the NREL buffer on GSE CIGS and IEC CdS. However, based on the results of NREL windows on GSE LT CdS and HT CdS, as well as the area limitations in the NREL RF ZnO sputter system, it must be speculated that the problem samples were not true window layer replicas and were deposited in a separate run yielding different, non-standard, i-ZnO/Al_2O_3:ZnO properties.

In summary, the data provides some confidence that there is room for improvement primarily in the GSE HT CdS buffer. Although the HT process has been modified in November of 2002, it is unclear as to whether or not it now rivals the LT CdS buffer. A separate HT vs. LT CdS comparison at GSE is thus underway. Some minor enhancements in the GSE window layer also appear possible and should be addressed in internal experiments.

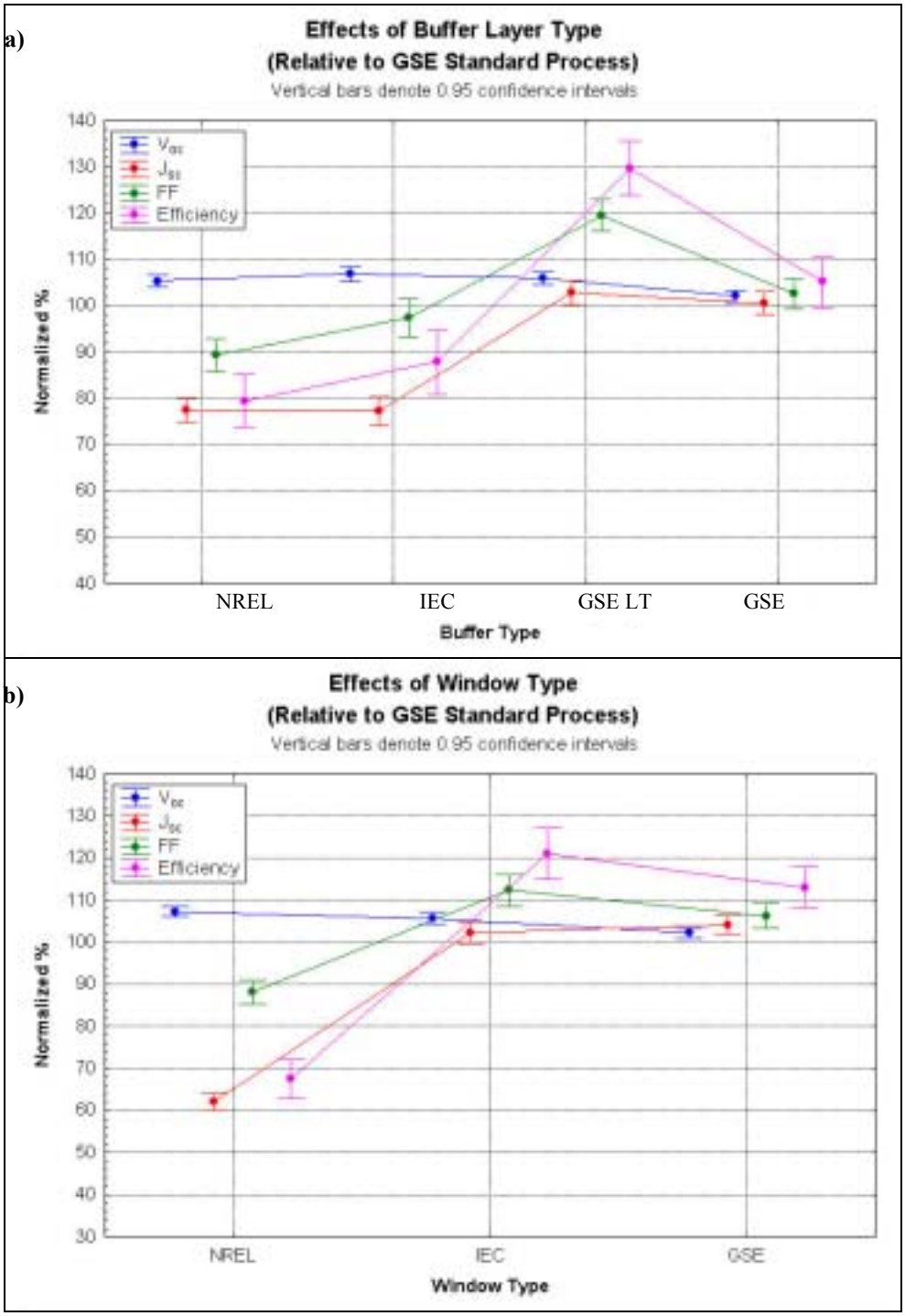

Figure 15: Device I-V parameter (Voc, Jsc, FF, η) estimates as a function of a) buffer and b) window layer compared to the GSE standard.

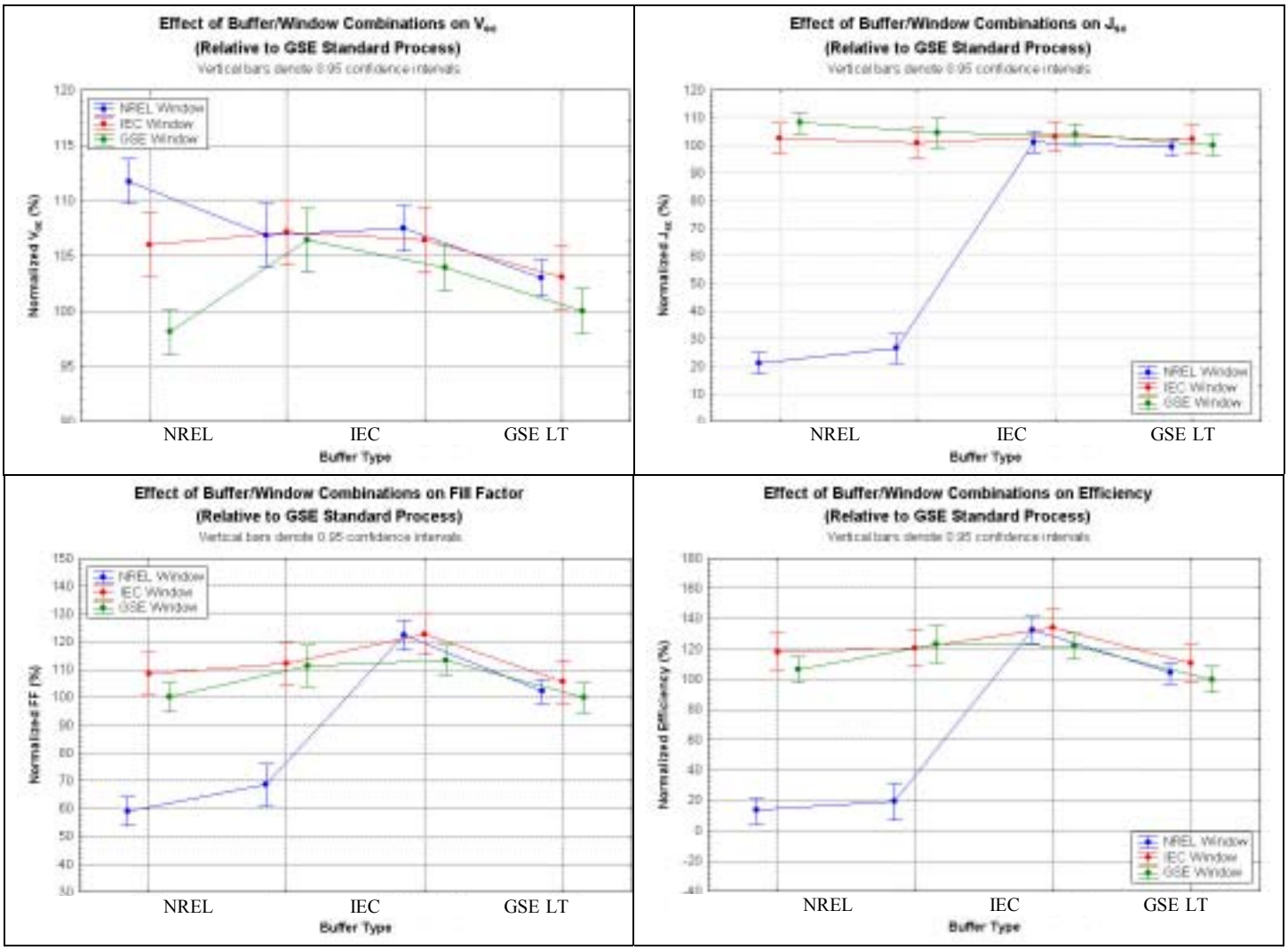

Figure 16: Device parameters measured on each permutation of buffer and window layer combinations.

3.e Se flux

Se flux as a function of position has been documented. The output of proprietary Se sensors was compared with Se fluxes calculated from Se feedstock usage, pumping speed, and film Se consumption. These two methods of Se flux estimation agree to within approximately a factor of two. Thus, Se fluxes in the roll-coater systems are known to within approximately a factor of two, and examinations in the bell jar will cover the corresponding envelope.

4 Three-Stage Sensitivities

The investigation three-stage process sensitivities began with an examination of the importance of the Cu-rich phase for CIS and CIGS films. Also, bell jar conditions relevant for the examination of instantaneous variations in Se to metals ratio were specified. These topics are described in following sub-sections in detail.

4.a Importance of Cu-rich stage

The effect of a Cu-rich phase in the three-stage growth process on device performance was examined for CIGS on glass. It was found that the Cu-rich phase is very important for good device performance when Ga is included in the films, but less so for CIS-only films. This conclusion differs from those reached by Shafarman[18,19] for a modified two-stage process and by Nishiwaki[20] for a three-stage process at unspecified deposition rates. Disparity of the conclusions suggests that the importance of the Cu-rich phase may be a strong function of temperature and flux profiles, as well as the overall deposition time. In the present case, a temperature of 575°C was monitored in the second stage by a contact thermocouple attached to the back of the substrate at a metal flux exposure span of 24 minutes.

The impact of the Cu-rich excursion was evaluated utilizing a composition gradient across the substrate. Due to the placement of the evaporation boats and sample, the 3" × 3" substrates used in this study exhibited a 12% gradient in Cu/(In+Ga) across the substrate. Thus, for example, in a film with a final Cu/(In+Ga) ratio of 0.9 at the center and 10% of the group III atoms introduced during the third stage, half of the substrate underwent a Cu-rich stage while the remaining half did not. The entire film, however, was within the composition range expected to produce high-efficiency devices as demonstrated by Gabor et al.[21] It should be noted that Gabor's data showing little sensitivity of device performance to composition in the range Cu/(In+Ga) = 0.86 to 0.92 is non-integral composition measured by electron probe microanalysis. It is therefore still possible that the Cu ratio very near the junction is the important variable for device performance, and may not always be the same as the integral Cu-ratio.

For CIGS films with Ga, the Cu-rich phase was found to be necessary for good device performance and large grains. In the following discussion, the side of the substrate that underwent a Cu-rich stage is labeled "*R*", and the side of the substrate that remained Cu-poor is labeled "*P*".

Current-voltage (JV) characteristics of devices representative of sides *R* and *P* on substrate B0209025-1 are shown in Figure 17. Device parameters are provided in the inset. The CIGS composition at the substrate center was determined at 0.94 and 0.26 for the Cu/(In+Ga) and Ga/(In+Ga) ratios, respectively. Efficiencies decreased gradually and monotonically across the substrate. Therefore, low efficiencies cannot be attributed to localized shunts from handling or debris.

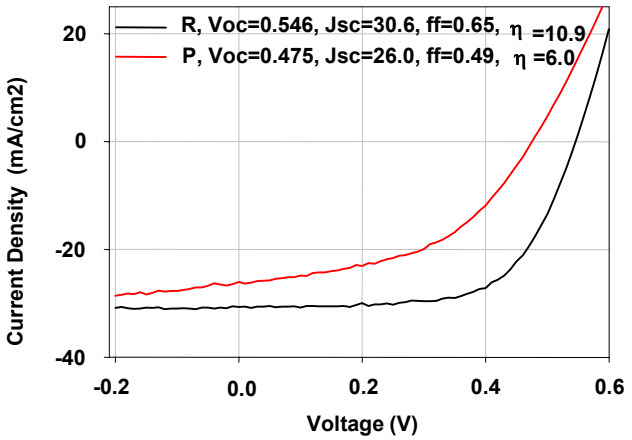

Figure 17: JV curves from side R and P of substrate.

A red loss in the *P* devices is evident from quantum efficiency (QE) measurements, being consistent with low diffusion lengths. QE is shown in Figure 18. The bump in the QE at 760 nm is an artifact seen in devices that display light-history dependent properties. The filter in the QE is switched before this data point, and the sample is momentarily exposed to bright white light. For cells with light-soaking dependent properties, a temporary increase in the QE is seen after this exposure.

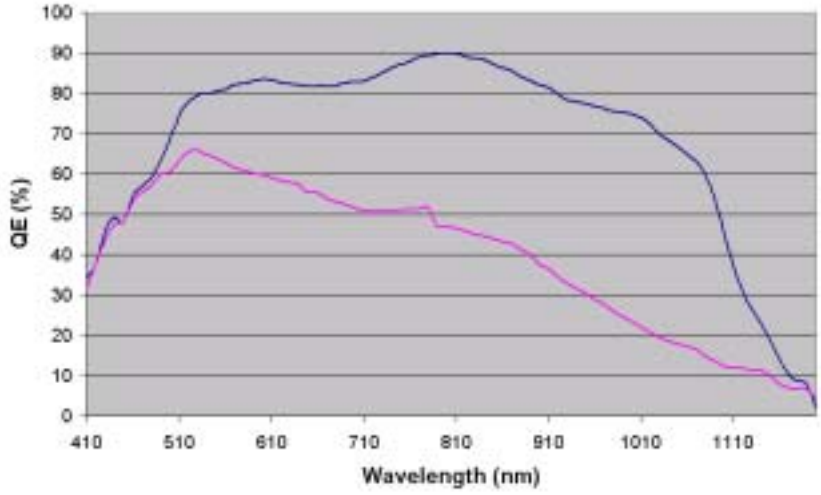

Figure 18: Quantum efficiency of devices from side R (blue) and P (pink).

With respect to morphology, the Cu-rich transition in the film was found to be associated with larger grains and a more densely-packed structure. Figure 19 illustrates SEM images of specimens *R* and *P*, as seen both from the surface and in cross-section. On side *R*, a large-grained structure is evident, while side *P* exhibits much smaller features. The cross-section micrograph of side *R* shows large features and a densely-packed film, while sample *P* exhibits much smaller features and more voids.

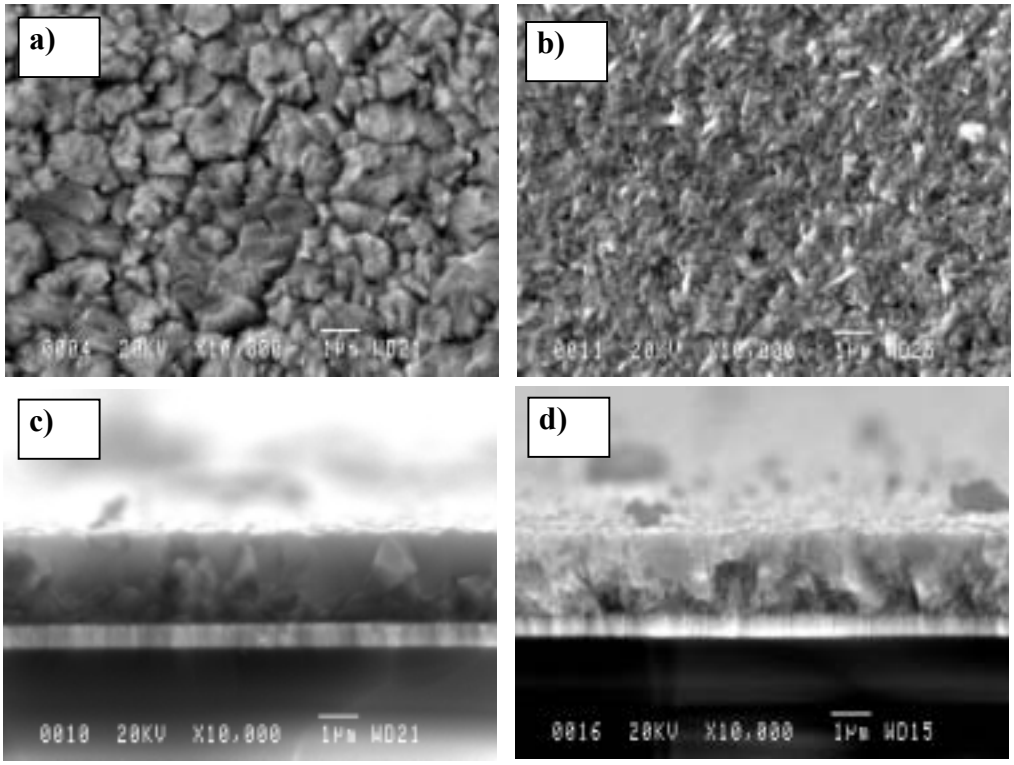

Figure 19: SEM images of a) surface R, b) surface P, c) cross-section R, and d) cross-section P.

The potential difference in device performance for the two groups of specimens due to different bandgap profiles can be excluded based on Auger emission spectroscopy (AES) depth profiling results, as plotted in Figure 20. The dotted lines indicate the composition for side *P*, while the solid lines represent the composition for side *R*. The compositional profiles are fairly uniform throughout the absorber thickness and similar for the two locations. Consistent with receiving less Cu, side *P* appears slightly thinner and has a lower relative Cu content, as well as a higher relative In content. AES was measured at NREL.

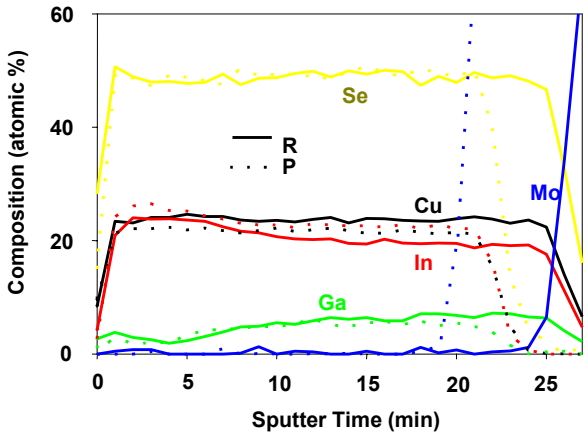

Figure 20: AES profiles for sides P (dotted) and R (solid).

In contrast, CIS device efficiency was found to be relatively insensitive to the existence of a Cu-rich growth period. For example, Figure 21 depicts device efficiency as a function of position over the center 30 cm^2 of substrate B020822. The average device efficiency is 7.9%, with a range spanning 6.8% to 8.7%. The Cu/(In+Ga) atomic ratio measured 0.85 at the substrate center. Thus, it has been demonstrated that the inclusion of Ga – although it allows for more efficient devices through better match of the absorber bandgap to the solar spectrum and the ITO transmission – also leads to a more sensitive process that requires a Cu-rich growth period, based on the parameter space explored here.

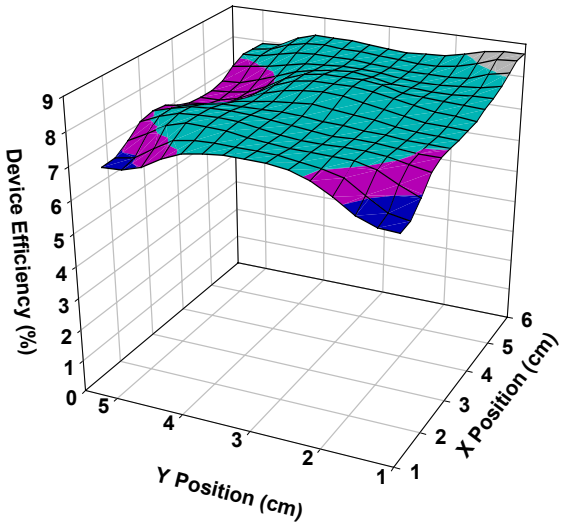

Figure 21: CIS device efficiency as a function of position on substrate B020822.

4.b Instantaneous Se-to-metals ratio

Flux profiles in the production roll coaters have been characterized to a degree that allows rough comparison with NREL three-stage profiles. The resulting comparison is shown in Figure 22. The bell jar flux profiles represent variations in flux encountered by the stationary substrate as changes are made to the source currents. The roll coater flux profiles represent the flux encountered by a point on the flexible substrate as it travels through the roll coater, with all source effusion rates held constant. In Figure 22, roll coater fluxes are graphed qualitatively, not to scale, in order to protect proprietary deposition setpoint and rate information.

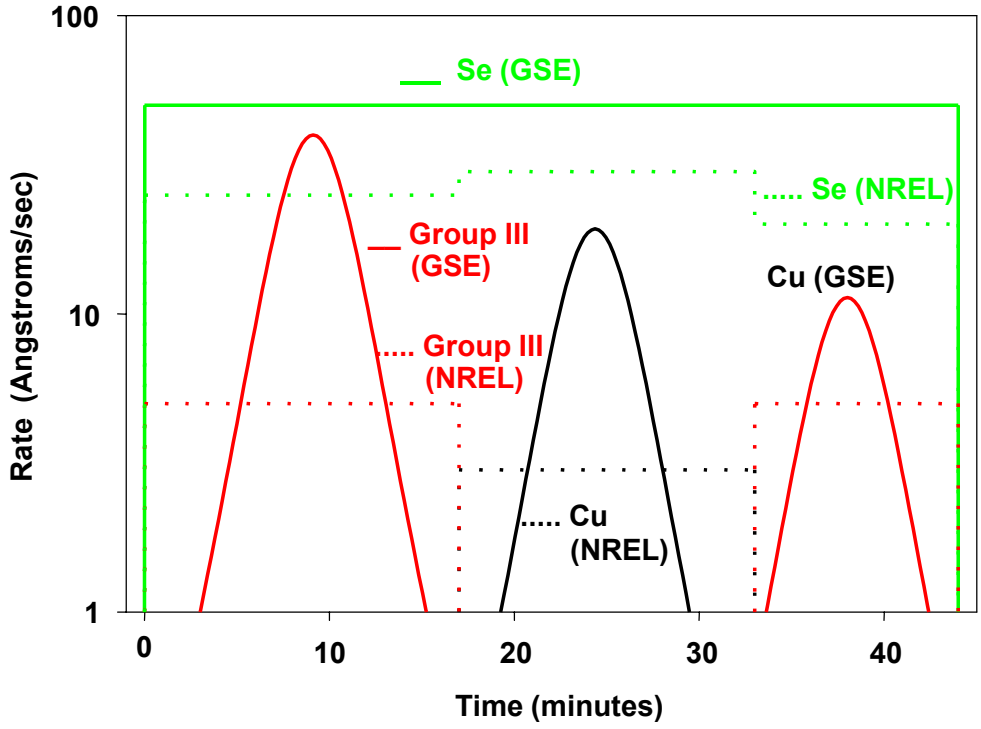

Figure 22: Standard three-stage bell jar rate profiles, and qualitative comparison with production roll-coater rate profiles.

Several features of Figure 22 deserve further examination. For the NREL rate profiles, Se to metals molar flux ratio is approximately constant and typically in excess of stoichiometry by a factor between 4 and 6. For the roll-coater flux profiles, the Se to metals molar flux ratio is sometimes less than that in the NREL recipe, and sometimes more. Also, even for films of the same thickness and same total deposition time deposited using the static three stage or roll-coater profiles, those deposited using the roll-coater profiles experience periods of growth at higher deposition rates than the static three-stage films. These observations suggest several modifications to the bell jar rate profiles to examine the sensitivity of the three-stage process to instantaneous Se/metals ratio and deposition rate. The automated system controlling metals rates as a function of time on the ITN bell jar was programmed to allow profiles like those shown in Figure 22. Rate control is achieved by electron impact emission spectroscopy rate monitoring in conjunction with computerized closed-loop control of the evaporation sources. An example of In and Cu stages with modified flux profiles are shown in Figure 23. These bell jar flux profiles imitate the roll-coater conditions of Figure 22. Standard, flat, bell jar flux profiles were shown earlier in Figure 7. Several adjustments to source programming are still necessary to create the desired smooth profiles. A suggested progression of bell jar metals flux profiles, for a constant Se rate, is shown in Figure 24. These suggested profiles deposit films of the same composition, thickness, and deposition time, but differing instantaneous deposition rates and Se/metals flux ratios.

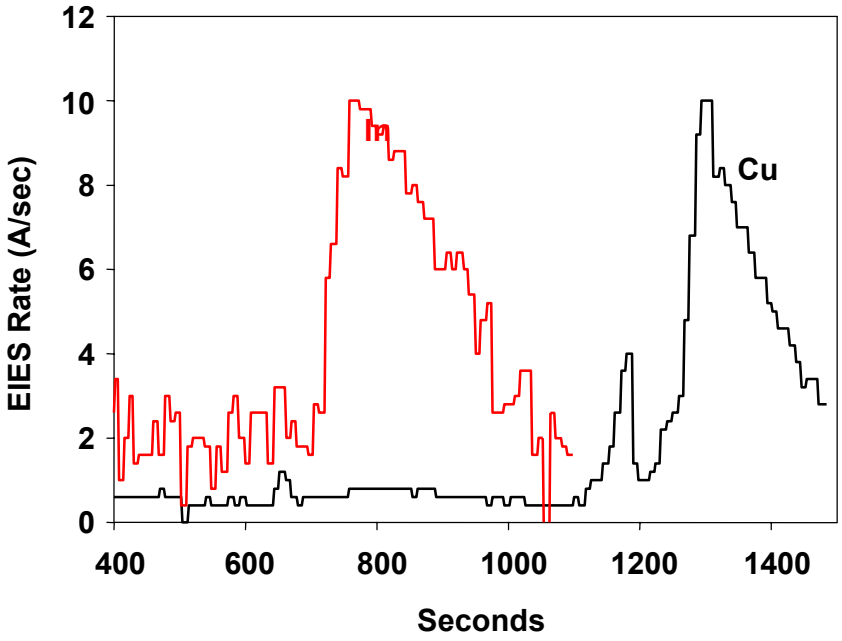

Figure 23: Bell jar In and Cu flux profiles imitating roll-coater conditions.

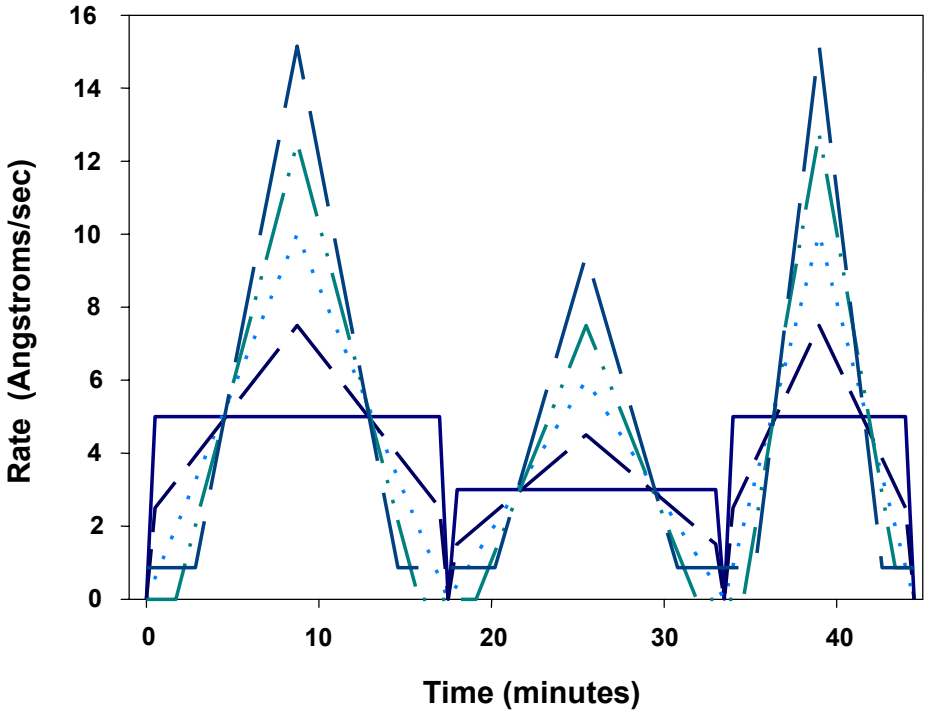

Figure 24: Progression of rate profiles for bell jar depositions.

5 Team Activities

GSE takes part in CIS National Team activities. Recent contributions have included participation in and presentations at team meetings, submission of samples for comparative absorber studies, and review and discussion of related data.

6 Summary

Several advancements were demonstrated during Phase I:

- A **baseline process** for examination of three-stage process sensitivities was established in a bell jar at ITN.
  - Best efficiencies (AM1.5, 1 cm^2, total area, no AR coating) are currently 9.3% for CIS on glass, 7.7% for CIS on production steel, and 10.9% for CIGS on glass.
  - NREL and ITN window layers produce nearly identical efficiencies when applied to the bell jar absorbers.
- Several aspects of the **production roll-coaters** were **characterized**.
  - Metals flux profiles agree well with a $\cos^3\theta$ dependence of the flux per solid angle.
  - The effect of Se pressure on the metals profiles is under examination.
  - Se flux was documented and results from two measurement methods agree within a factor of 2.
  - Uniformity of CdS solution temperature in a reaction vessel was improved.
  - Small-area devices on absorbers were finished at NREL, IEC, and in the GSE production roll coaters, yielding similar results. Some minor enhancements in the GSE high throughput window layers appear possible and will be addressed.
- Examination of **three-stage process sensitivities** began in the bell jar.
  - For Ga-containing absorbers, the Cu-rich phase is very important to achieve good device performance.
  - Cu-rich growth is less important for CIS-only films.
  - Given the disparity of this conclusion with work in the literature for slightly different recipes, it is likely that the importance of the Cu-rich phase is a strong function of temperature and flux profiles, as well as the overall deposition time.
  - Low efficiencies in Ga-containing devices not undergoing a Cu-rich transition are correlated with small CIGS grain size.
  - To carefully control the extent of the Cu-rich excursion, IR emissivity monitoring was implemented.
  - Bell jar conditions relevant for the examination of instantaneous variations in Se to metals ratio were specified.
  - Metals fluxes versus time imitating those in the roll coaters were demonstrated in the bell jar.

7 Future Directions

During Phase I, work focused on establishing the three-stage bell jar process, characterizing the metals and Se fluxes in the production roll coaters, and quantifying the contribution of the production window layers toward efficiency loss and variability. Some initial three-stage process sensitivities were examined in the bell jar.

Phase II tasks will build on this year's results. In the bell jar, emphasis will shift from baseline verification to investigation of more involved process sensitivities. These investigations will include use of less expensive source materials, decreased deposition times, variations in instantaneous Se to metals ratio as implied by the roll coater flux profiles, variations in the fraction of group III elements deposited in the third stage, modifications to sample cool-down temperature and Se profiles, variations in first and second stage temperatures, exposure of the substrate to reflected hot-wall species, and different times stored at atmosphere or dry N_2 environment between CIGS and CdS depositions. Minor refinements to the baseline will be implemented as appropriate. In the production roll-coaters, characterization will be extended to the more difficult quantities of temperature and of metals profiles with Se pressure. The Phase II tasks lead

toward third-year goal of applying process sensitivity information in the production roll-coaters and demonstrating process improvement.

8 References

[1] J.R. Tuttle, M.A. Contreras, K.R. Ramanathan, S.E. Asher, R. Bhattacharya, T.A. Berens, J. Keane, R. Noufi, "Materials and Processing Issues in Thin-Film Cu(In,Ga)Se_2□Based Solar Cells", *AIP Conference Proceedings 394*, 83-105 (1996).

[2] Hedstrom, H. Ohlsen, M. Bodegard, A. Kylner, L. Stolt, D. Hariskos, M. Ruckh, H.W. Schock, *Proceedings of the 23rd IEEE Photovoltaics Specialists Conference*, 364-371 (1993).

[3] W.N. Shafarman, R.W. Birkmire, M. Marudachalam, B.E. McCandless, J.M. Schultz, "Fabrication and Characterization of Cu(In,Ga)Se2 Solar Cells with Absorber Bandgap from 1.0 to 1.5 eV", *AIP Conference Proceedings 394*, 123-131 (1996).

[4] T. Wada, S. Hayashi, Y. Hashimoto, S. Nishiwaki, T. Sato, T. Negami, M. Nishitani, "High Efficiency Cu(In,Ga)Se_2 (CIGS) Solar Cells with Improved CIGS Surface", *Proceedings of the 2nd World Conference and Exhibition on Photovoltaic Energy Conversion*, pp. 403-408, 1998.

[5] B. Dimmler, E. Gross, D. Hariskos, F. Kessler, E. Lotter, M. Powalla, J. Springer, U. Stein G. Voorwinden, M. Gaeng, S. Schleicher, "CIGS Thin Film Module Technology: Towards Commercialization", *Proceedings of the 2nd World Conference and Exhibition on Photovoltaic Energy Conversion*, pp. 419-423, 1998.

[6] W.N. Shafarman, R.W. Birkmire, S. Marsillac, M. Marudachalam, N. Orbey, T.W.F Russell, "Effect of Reduced Deposition Temperature, Time, and Thickness, on Cu(In,Ga)Se_2 Films and Devices", *Conference Record of the 25th IEEE Photovoltaic Specialists Conference*, pp.331-334, (1996).

[7] W.N. Shafarman, J. Zhu, "Effect of Substrate Temperature and Deposition Profile on Evaporated Cu(In,Ga)Se_2 films and devices", *Thin Solid Films* **361-362**, pp. 473-477, (2000).

[8] S. Nishiwaki, T. Satoh, S. Hayashi, Y. Hashimoto, T. Negami, T. Wada, "Preparation of Cu(In,Ga)Se_2 thin films from In-Ga-Se Precursors for high-efficiency solar cells", *Journal of Materials Research* **14** (12), pp. 4514-4520, (1999).

[9] J.R. Tuttle, T.A. Berens, J. Keane, K.R. Ramanathan, J. Granata, R.N. Bhattacharya, H. Wiesner, M.A. Contreras, R. Noufi, "Investigations into Alternate Substrate, Absorber, and Buffer Layer Processing for Cu(In,Ge)Se_2 – Based Solar Cells", *Conference Record of the 25th IEEE Photovoltaic Specialists Conference*, pp.797-800, (1996).

[10] J.E. Granata, "The Impact of Deliberate Sodium Incorporation on $CuInSe_2$-Based Solar Cells", Unpublished Ph.D. Thesis, Colorado State University, (1999).

[11] A.M. Gabor, J.R. Tuttle, D.S. Albin, M.A. Contreras, R. Noufi, A.M. Herman, "High-efficiency $CuIn_xGa_{1-x}Se_2$ solar cells made from $(In_x,Ga_{1-x})_2Se_3$ precursor films", *Applied Physics Letters*, **65**(2), pp. 198-200, (1994).

[12] J. Kessler, J. Scholdstrom, L. Stolt, "Rapid Cu(In,Ga)Se_2 Growth Using 'End Point Detection' ", *Proceedings of the 28th IEEE Photovoltaics Specialists Conference*, (2000).

[13] T.S. Satoh, S. Hayashi, S. Nishiwaki, S. Shimkawa, Y. Hashimoto, T. Negami, T. Uenoyama, "Fabrication of Cu(In,Ga)Se_2 by In-Line Evaporation (Composition Monitoring Method Using Heat Radiation)", *Solar Energy Materials and Solar Cells* **67**, 2001, pp. 203-207.

[14] M. Nishitani, T. Negami, T. Wada, "Composition Monitoring Method in $CuInSe_2$ Thin Film Preparation", *Thin Solid Films* **258**, 1995, pp. 313-316.

[15] T. Negami, M. Nishitani, N. Kohara, Y. Hashimoto,T. Wada, "Real-Time Composition Monitoring Methods In Physical Vapor Deposition of Cu(In,Ga)Se_2 Thin Films", *Materials Research Society Symposium Proceedings* **Vol. 67**, 1996, pp. 267-278.

[16] R.W. Birkmire, W.N. Shafarman, E. Eser, S.S. Hegedus, B.E. McCandless, R. Aparicio, K. Dobson, "Optimization of Processing and Modeling Issues for Thin Film Solar Cell Devices Including Concepts for the Development of Polycrystalline Multijunctions", *Annual Report to NREL under Subcontract ZAK-8-17619-33*, 2001, pp. 3-4.

[17] NREL PVMat Subcontract ZDO-2-30628-07, "Trajectory Oriented and Fault Tolerant Based, Intelligent Process Control for Flexible CIGS PV Module Manufacturing", in progress.

[18] W.N. Shafarman, R.W. Birkmire, S. Marsillac, M. Marudachalam, N. Orbey, T.W.F Russell, "Effect of Reduced Deposition Temperature, Time, and Thickness, on Cu(In,Ga)Se_2 Films and Devices", *Conference Record of the 25th IEEE Photovoltaic Specialists Conference*, (1996), pp.331-334.

[19] W.N. Shafarman, J. Zhu, "Effect of Substrate Temperature and Deposition Profile on Evaporated Cu(In,Ga)Se_2 films and devices", *Thin Solid Films* **361-362**, (2000), pp. 473-477.

[20] S. Nishiwaki, T. Satoh, S. Hayashi, Y. Hashimoto, T. Negami, T. Wada, "Preparation of Cu(In,Ga)Se_2 thin films from In-Ga-Se precursors for high-efficiency solar cells", *Journal of Materials Research* **14** (12) , (1999), pp. 4514-4520.

[21] A.M. Gabor, J.R. Tuttle, D.S. Albin, M.A. Contreras, R. Noufi, A.M. Herman, "High-efficiency $CuIn_xGa_{1-x}Se_2$ solar cells made from $(In_x,Ga_{1-x})_2Se_3$ precursor films", *Applied Physics Letters*, **65**(2), (1994), pp. 198-200.

REPORT DOCUMENTATION PAGE

Form Approved
OMB NO. 0704-0188

1. AGENCY USE ONLY (Leave blank)	2. REPORT DATE	3. REPORT TYPE AND DATES COVERED
	June 2003	Phase I Annual Report May 2002–May 2003

4. TITLE AND SUBTITLE
Tolerance of Three-Stage CIGS Deposition to Variations Imposed by Roll-to-Roll Processing: Phase I Annual Report, May 2002–May 2003

5. FUNDING NUMBERS
PVP35001
ZDJ-2-30630-14

6. AUTHOR(S)
M.E. Beck and I.L. Repins

7. PERFORMING ORGANIZATION NAME(S) AND ADDRESS(ES)
Global Solar Energy, Inc.
5575 South Houghton Road
Tucson, Arizona 85747
and
ITN Energy Systems, Inc.
8130 Shaffer Parkway
Littleton, Colorado 80127

8. PERFORMING ORGANIZATION REPORT NUMBER

9. SPONSORING/MONITORING AGENCY NAME(S) AND ADDRESS(ES)
National Renewable Energy Laboratory
1617 Cole Blvd.
Golden, CO 80401-3393

10. SPONSORING/MONITORING AGENCY REPORT NUMBER
NREL/SR-520-34314

11. SUPPLEMENTARY NOTES
NREL Technical Monitor: Harin S. Ullal

12a. DISTRIBUTION/AVAILABILITY STATEMENT
National Technical Information Service
U.S. Department of Commerce
5285 Port Royal Road
Springfield, VA 22161

12b. DISTRIBUTION CODE

13. ABSTRACT *(Maximum 200 words):* Global Solar Energy, Inc. (GSE) and subcontractor ITN Energy Systems, Inc. (ITN) are addressing process tolerance issues in this program. The definition and resolution of process tolerance issues satisfy many of the goals of the Thin Film Photovoltaics Partnership Program (TFPPP). First, the investigation is likely to identify acceptable ranges for critical deposition parameters. This will have the benefit of providing upper and lower control limits for in-situ process-monitoring components, thus increasing average efficiency, as well as yield of product. Second, the exploration may uncover insensitivities to some processing procedures, allowing manufacture of modules at increased throughput and decreased cost. The exploration allows a quantitative evaluation of the trade-offs between performance, throughput, and costs. Third, the proposed program also satifies the TFPPP goal of establishing a wider research and development base for higher-efficiency processing. Fourth, the acquisition of data defining sensitivity to processing has important implications for the required accuracy of process sensors and control. Finally, the program helps the photovoltaic community advance toward a better understanding of CIGS growth, which is a longer-term goal of the TFPPP.

14. SUBJECT TERMS: PV; bell jar baseline; roll-coater conditions; three-stage; metal fluxes; process sensitivity

15. NUMBER OF PAGES

16. PRICE CODE

17. SECURITY CLASSIFICATION OF REPORT	18. SECURITY CLASSIFICATION OF THIS PAGE	19. SECURITY CLASSIFICATION OF ABSTRACT	20. LIMITATION OF ABSTRACT
Unclassified	Unclassified	Unclassified	UL